

Relationships Between Stellar Velocity Dispersion and the Atmospheres of Early-Type Galaxies

RACHEL L.S. FRISBIE,¹ MEGAN DONAHUE,¹ G. MARK VOIT,¹ KIRAN LAKHCHAURA,² NORBERT WERNER,³ AND MING SUN⁴

¹*Physics and Astronomy Department, Michigan State University, East Lansing, MI 48824-2320, USA*

²*MTA-ELTE Astrophysics Research Group, Pázmány Péter sétány 1/A, Budapest, 1117, Hungary*

³*Department of Theoretical Physics and Astrophysics, Faculty of Science, Masaryk University, Kotlářská 2, Brno, 602 00, Czech Republic*

⁴*Department of Physics and Astronomy, University of Alabama in Huntsville, Huntsville, AL 35899, USA*

ABSTRACT

The Voit et al. (2020) black hole feedback valve model predicts relationships between stellar velocity dispersion and atmospheric structure among massive early-type galaxies. In this work, we test that model using the Chandra archival sample of 49 early-type galaxies from Lakhchaura et al. (2018). We consider relationships between stellar velocity dispersion and entropy profile slope, multiphase gas extent, and the ratio of cooling time to freefall time. We also define subsamples based on data quality and entropy profile properties that clarify those relationships and enable more specific tests of the model predictions. We find that the atmospheric properties of early-type galaxies generally align with the predictions of the Voit et al. (2020) model, in that galaxies with greater stellar velocity dispersion tend to have radial profiles of pressure, gas density, and entropy with steeper slopes and less extended multiphase gas. Quantitative agreement with the model predictions improves when the sample is restricted to have low central entropy and stellar velocity dispersion of between 220 and 300 km s⁻¹.

1. INTRODUCTION

Early-type galaxies, encompassing both elliptical and lenticular galaxies, are characterized by their elliptical shapes, older stellar populations, and lack of significant active star formation. Star formation in galaxies occurs when there is sufficient molecular gas to form stars and proceeds until the molecular gas supply runs out, either through stars forming more rapidly than the molecular gas can accumulate or the galaxy preventing further accumulation of molecular gas. It follows then, because little star formation is observed in early-type galaxies, that those galaxies must be preventing molecular gas from accumulating. Molecular gas can accumulate in galaxies via cold streams (e.g. Kereš et al. 2005, 2009; Dekel et al. 2009), cooling flows (e.g. White & Frenk 1991; Fabian 1994; McNamara & Nulsen 2007, 2012; Werner et al. 2019), stellar mass loss (e.g. Mathews & Brighenti 2003; Leitner & Kravtsov 2011; Voit & Donahue 2011), or perhaps tidal interactions with other galaxies. Therefore, feedback processes in early-type galaxies must limit those gas sources.

The effects of feedback processes on galactic atmospheres can be probed through observations of the hot X-ray emitting gas. One way feedback alters the rate at which gas flows into a galaxy is by affecting the cooling time of its atmospheric gas. For example, adding heat to a galactic atmosphere raises its entropy. If the heating

due to feedback is gradual compared to the time it takes for the heated gas to expand within the gravitational potential, the temperature of the atmosphere may not change much while its density declines and its cooling time lengthens. Entropy is therefore the preferred quantity for investigating feedback processes and is represented in this paper by the entropy index $K \equiv kTn_e^{-2/3}$, where kT is gas temperature and n_e is electron density. We define the cooling time (t_{cool}) of the gas to be the time needed for gas at temperature T to radiate an energy $3kT/2$ per particle. For an atmosphere near hydrostatic equilibrium, the sound-crossing time required for heating to drive expansion is similar to the freefall time $t_{\text{ff}} = (2r/g)^{1/2}$, defined with respect to the local gravitational acceleration g at galactocentric radius r . A galactic potential well serves as an entropy sorting device, causing lower entropy gas to sink, while higher entropy gas rises to larger radii. The atmosphere's lowest entropy gas therefore collects near the center, where it is the densest and brightest X-ray emitting gas in the galaxy.

Voit et al. (2015) examined the properties of a sample of 10 massive elliptical galaxies previously studied by Werner et al. (2012, 2014) and showed that the entropy profile slopes of early-type galaxies correlate with the presence of multiphase gas in that small sample. The gas entropy levels of those galaxies are similar inside the

central ~ 2 kpc, but their entropy profile slopes outside of ~ 2 kpc differ. Galaxies with extended multiphase gas exhibit entropy profiles with $K \propto r^{2/3}$ at ~ 1 – 10 kpc while galaxies with no extended multiphase gas (hereafter referred to as single phase galaxies) exhibit steeper entropy profiles, with $K \propto r$ at ~ 1 – 10 kpc.

Voit et al. (2015) hypothesized that the differences in the entropy profile slope could be due to supernova (SN) type Ia heating that sweeps gas ejected by the old stellar population out of a single phase galaxy into an extended gaseous halo. They also found that the velocity dispersions of the galaxies with extended multiphase gas were $\sigma_v \leq 255$ km s $^{-1}$ while galaxies with no extended multiphase gas had $\sigma_v \geq 263$ km s $^{-1}$. How a black hole interacts with a galactic atmosphere, as reflected by its entropy profile slope and multiphase gas extent, therefore appears to be related to the galaxy’s velocity dispersion.

Lakhchaura et al. (2018) explored the relationship between entropy profile slope and multiphase gas extent in a larger archival sample (~ 50 galaxies) but did not report evidence for a relationship. However, Lakhchaura et al. (2018) did find evidence for a relationship between the average behavior of entropy profiles and the atmospheric ratio of cooling time to freefall time. Babyk et al. (2018) explored the relationship between entropy profile slope and velocity dispersion for an archival sample of 40 early-type galaxies (and 110 clusters). They did not report evidence for a relationship between entropy profile slope and velocity dispersion but did find some evidence for a relationship between entropy profile slope and atmospheric temperature.

Voit et al. (2020) modeled the coupling between supernova sweeping of stellar ejecta, the confining circumgalactic medium (CGM) pressure, and bipolar kinetic feedback fueled by accretion of cooling gas onto the central black hole, and showed how it forms a “black hole feedback valve.” They presented an analytic model that predicts a simple relationship between a galaxy’s stellar velocity dispersion and its entropy profile slope, based on how SN Ia heating affects a galactic atmosphere and the locations where multiphase gas tends to form. The model is informed by both numerical simulations and observations and predicts the entropy profile slope within the radial range (~ 1 – 10 kpc) in which SN Ia heating is capable of exceeding radiative cooling. If SN Ia heating does exceed radiative cooling there, then the entropy profile slope of the atmosphere in that region is determined by the ratio of the specific thermal energy of the ejected stellar gas to the depth of the galactic potential well, as long as the outflow that heating drives is subsonic.

The structure of this paper is as follows. Section 2 describes our sample selection and data analysis procedures. Section 3 compares the model predictions of Voit et al. (2020) with those observations. Section 4 concludes by discussing how this work relates to the current understanding of precipitation-driven feedback in massive galaxies.

2. METHODS

2.1. Sample Description

Our primary goal in this work is to determine whether the model predictions from Voit et al. (2020) are consistent with the observed relationships between stellar velocity dispersion and atmospheric entropy profile slope. Making such a comparison requires observations with sufficient resolution to measure an entropy profile slope, so we need to use a sample of early-type galaxies with accurate entropy profiles and velocity dispersion measurements to test the model’s predictions.

The galaxies explored in this work were drawn from an analysis by Lakhchaura et al. (2018) of 49 nearby, X-ray and optically bright, elliptical galaxies with archival Chandra data. We adopted the radial profile measurements of electron density n_e , temperature kT , specific entropy K , and the cooling time to freefall time ratio t_c/t_{ff} from Lakhchaura et al. (2018), as well as their classification scheme for the extent of multiphase gas. However, we restricted our analysis to a high-quality (HQ) subsample with a spatial resolution sufficient to fit a three-parameter entropy profile model in the 1 – 10 kpc range (see §2.4 for details).

Table 1 lists the properties of the galaxies in the HQ subsample. According to the Lakhchaura et al. (2018) classification scheme, extended-emission (E) galaxies have optical line emission extending to more than 2 kpc from the center, nuclear-emission (NE) galaxies have line emission confined to the central 2 kpc, no-emission (N) galaxies have no detectable optical line emission, and U galaxies have unknown line-emission characteristics. The σ_v values in Table 1 are from the HYPERLEDA database.¹ The cooling time t_{cool} is calculated from the X-ray observations assuming solar metallicity, and the estimated freefall time is taken to be $t_{\text{ff}} = \sigma_v/r$.

Many of the emission-line classifications in Lakhchaura et al. (2018) were based on long-slit spectroscopy collected at the SOAR and Apache Point (APO) observatories, to be described in papers still in preparation. The SOAR observations come from the Goodman High-Throughput Spectrograph using

¹ <http://leda.univ-lyon1.fr>

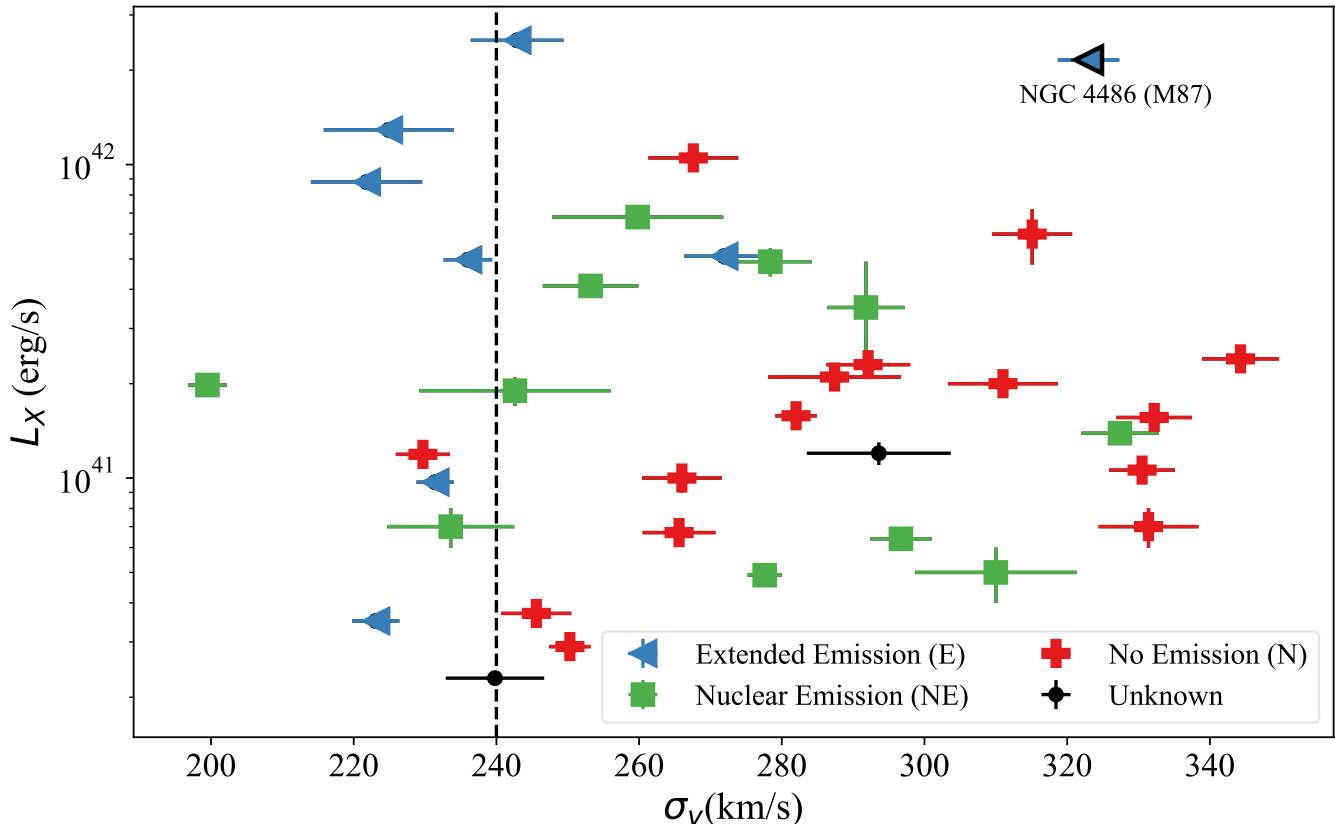


Figure 1. Stellar velocity dispersion (σ_v) vs. X-ray luminosity (L_X) from within the central 10 kpc of an early-type galaxy. The figure shows our high-quality (HQ) subsample of galaxies from Lakhchaura et al. (2018) that have data quality sufficient for us to measure an accurate entropy profile slope at 1–10 kpc. Blue triangles represent galaxies with extended multiphase gas (E), red crosses represent galaxies with no extended multiphase gas (N), green squares represent galaxies with multiphase gas contained within 2 kpc (NE), and black dots represent galaxies without a multiphase gas classification from Lakhchaura et al. (2018). A vertical dashed line indicates the velocity dispersion (240 km s⁻¹) that the Voit et al. (2020) model predicts should correspond to the critical entropy profile slope of $K \propto r^{2/3}$.

the 1''68 slit and the 600 l/mm grating. They cover $\sim 2600 \text{ \AA}$, with an approximate spectral resolution of $R \sim 800$ at a central wavelength of 6000 \AA . The APO observations come from the Dual Imaging Spectrograph using the 2'' slit and the R1200/B1200 grating. They cover $\sim 1200 \text{ \AA}$, with an approximate spectral resolution of $R \sim 900$ at a central wavelength of 6600 \AA .

The Lakhchaura et al. (2018) classifications should not be considered definitive, because the data sets on which they are based are inhomogeneous, with differing sensitivities and equivalent width limits. Future observations of greater sensitivity may therefore shift galaxies from the N class into the NE class, or from the NE class into the E class. However, we are retaining those classifications here, with one exception,² so that the results of this

paper can be compared directly with those presented in Lakhchaura et al. (2018).

Figure 1 shows the relationships between X-ray luminosity, stellar velocity dispersion, and multiphase gas characteristics for galaxies in the HQ subsample. Voit et al. (2020) argued that the atmospheric properties of such galaxies should change above $\sigma_v = 240 \text{ km s}^{-1}$, at which the analytical model they present predicts an entropy profile $K \propto r^{2/3}$ for reasons outlined in §2.2. In the HQ subsample, extended multiphase gas appears to be more common among galaxies with $\sigma_v \lesssim 240 \text{ km s}^{-1}$ than among those with $\sigma_v > 250 \text{ km s}^{-1}$. Figure 1 also shows that galaxies with multiphase gas confined to the inner $\sim 2 \text{ kpc}$ are represented across the full range of σ_v . The most notable exception to the tendency for galaxies with greater σ_v to lack extended multiphase gas is M87 (also known as NGC 4486), which has an H α nebula extending several kiloparsecs from the center (e.g., Sparks et al. 2004; Boselli et al. 2019). It is the only

² We have corrected the Lakhchaura et al. (2018) classification of IC 4296, shifting it from NE to E, for reasons described in Frisbie et al. (2020).

galaxy in the upper right of Figure 1, it resides in one of the most massive halos in the sample, and it has one of the greatest X-ray luminosities within 10 kpc. The large luminosity from that inner region results from high external gas pressure, applied by overlying gas in this halo. The atmospheric characteristics of M87 are therefore representative of the entire massive halo rather than the potential well of this single galaxy.

Apart from M87, the upper envelope of L_X in Figure 1 exhibits a decline with increasing velocity dispersion. This feature is consistent with the hypothesis of Voit et al. 2015, 2020, which predicts that galaxies with greater velocity dispersions should have steeper entropy profile slopes. A steeper entropy profile slope means that the typical electron density within 10 kpc (the aperture for measuring L_X) is generally smaller than it would be for a shallower entropy profile slope.

Section 2.4 will discuss some smaller subsets of the Lakhchaura et al. (2018) sample that help to further refine our tests of the model predictions.

2.2. Model Predictions

Voit et al. (2020) presented a simple analytical prediction for the relationship between entropy profile slope ($\alpha_K \equiv d \ln K / d \ln r$) and stellar velocity dispersion (σ_v) in an early-type galaxy. The basic model assumes that the galaxy’s stellar mass distribution can be approximated by a singular isothermal sphere (constant circular velocity v_c) with a one-dimensional velocity dispersion $\sigma_v = v_c / \sqrt{2}$. If SN Ia heating locally dominates radiative cooling and black hole feedback, then it will drive an outflow that is subsonic within the galaxy, and therefore close to hydrostatic equilibrium. The radial power-law slopes of pressure, density, and entropy in such an outflow depend on how the specific energy of the gas compares with the gravitational potential. If gravity is insignificant, those power-law slopes will be shallow, but if the gravitational potential energy is comparable to the thermal energy, then those slopes will be steep. Consequently, outflows driven by stellar heating from galaxies with deeper central potentials, corresponding to larger σ_v , should have profiles of pressure, density, and entropy that are more centrally concentrated and focus radiative cooling more tightly around the central black hole.

Combining the contributions to the entropy profile from supernova energy, stellar orbital energy, and gravitational potential energy gives the following quantitative prediction for the relationship between α_K and v_c :

$$\alpha_K \approx \frac{5}{3} \left(\frac{\epsilon_*}{v_c^2} - \frac{1}{4} \right)^{-1}, \quad (1)$$

where ϵ_* is the mean specific energy of the gas coming from stars, including SN Ia heating, which amounts to ≈ 2 keV per particle for reasons outlined in Voit et al. (2020). Therefore, the structure of the galaxy’s atmosphere at 1–10 kpc depends strongly on ϵ_*/v_c^2 , which is equivalent to $\epsilon_*/2\sigma_v^2$. Section 3.1 compares this prediction with the HQ subsample.

Voit et al. (2020) also presented a slightly more realistic form of the basic model, assuming that the galaxy’s halo has a Navarro-Frenk-White (NFW) density profile and the stellar mass density follows a modified Einasto profile. Numerical integration of the more realistic model shows that the basic model overpredicts the entropy profile slope for $\sigma_v > 300$ km s⁻¹. We compare that modification of the basic model with the HQ subsample in §3.2.

2.3. Entropy Profile Measurements

Equation 1 is based on a steady, pressure bounded, subsonic outflow solution, heated only by SN Ia in an isothermal potential, and predicts a constant value of α_K in the region where those conditions apply. Because we want to test that prediction for the relationship between α_K and σ_v , we limit the range over which we fit α_K to the radial range that is affected as little as possible by other heating processes.

If feedback from the active galactic nucleus (AGN) is as powerful as in NGC 4261 and IC 4296 (see Frisbie et al. 2020), it typically deposits its energy rather far from the center ($r > 10$ kpc) because its jets drill through the hot gas, allowing stellar heating to dominate at smaller radii. However, a fraction of that AGN energy output might couple to gas closer to the AGN in some galaxies, resulting in a flattening or even an inversion of the entropy profile near 1 kpc. Therefore, we limit our entropy profile slope measurements to 1–10 kpc to get a “clean” measure of α_K where stellar processes are most likely to dominate.

While a few of the galaxies in our sample have entropy profiles that resemble a pure power law (Frisbie et al. 2020), most have an excess of entropy over a pure power law in the central kiloparsec. Therefore, we have adapted the functional form used by Donahue et al. (2005, 2006) and Cavagnolo et al. (2008) to a radial range more appropriate for individual galaxies instead of galaxy clusters:

$$K(r) = K_0 + K_{10} \left(\frac{r}{10 \text{ kpc}} \right)^{\alpha_K}, \quad (2)$$

where K_0 is a constant core entropy, K_{10} is the normalization of the power-law component at a radius of 10 kpc, and α_K is the best-fitting power-law slope.

Table 1. Properties of the HQ Subsample of Galaxies from Lakhchaura et al. (2018)

Galaxy	z	D (Mpc)	σ_v (km s^{-1})	L_X (10^{42}erg s^{-1})	Emission Extent	α_K	$\min(t_c/t_{\#})$	K_0 (keV cm^2)
(1)	(2)	(3)	(4)	(5)	(6)	(7)	(8)	(9)
IC1860	0.0229	95.75	259.8 ± 12.0	0.68 ± 0.050	NE ^a	0.66 ± 0.24	18.42 ± 2.40	5.92 ± 0.97
IC4296	0.0124	47.31	327.4 ± 5.4	0.14 ± 0.003	NE ^a	1.23 ± 0.11	11.63 ± 0.78	0.69 ± 0.20
IC4765	0.0150	59.52	278.4 ± 5.8	0.49 ± 0.050	NE ^a	0.88 ± 0.22	11.01 ± 1.20	1.82 ± 0.72
NGC315	0.0164	56.01	293.6 ± 10.1	0.12 ± 0.010	U	0.83 ± 0.24	20.02 ± 4.65	0.91 ± 0.96
NGC410	0.0176	66.00	291.8 ± 5.4	0.35 ± 0.140	NE ^b	0.76 ± 0.35	27.30 ± 5.22	4.93 ± 1.36
NGC499	0.0147	60.74	253.2 ± 6.7	0.41 ± 0.030	NE ^b	0.74 ± 0.24	34.18 ± 3.19	6.90 ± 4.16
NGC507	0.0164	59.83	292.1 ± 5.9	0.23 ± 0.020	N ^b	0.80 ± 0.34	30.15 ± 5.61	7.14 ± 3.38
NGC533	0.0184	61.58	271.9 ± 5.6	0.51 ± 0.030	E ^{a,d}	0.88 ± 0.14	12.28 ± 3.75	1.74 ± 0.36
NGC708	0.0162	64.19	221.8 ± 7.8	0.88 ± 0.020	E ^c	0.64 ± 0.06	12.04 ± 0.29	5.38 ± 0.15
NGC741	0.0186	64.39	287.4 ± 9.3	0.21 ± 0.010	N ^{a,b}	0.93 ± 0.09	19.16 ± 0.73	2.57 ± 0.39
NGC777	0.0167	58.08	315.1 ± 5.6	0.60 ± 0.120	N ^b	0.59 ± 0.24	24.11 ± 3.01	5.22 ± 1.01
NGC1316	0.0059	19.25	223.1 ± 3.3	0.04 ± 0.002	E ^a	0.72 ± 0.25	32.57 ± 6.72	0.58 ± 0.61
NGC1399	0.0048	17.75	332.2 ± 5.3	0.16 ± 0.004	N ^a	0.94 ± 0.03	26.05 ± 0.40	0.89 ± 0.11
NGC1404	0.0065	19.18	229.7 ± 3.8	0.12 ± 0.001	N ^a	0.80 ± 0.03	20.23 ± 0.51	0.70 ± 0.04
NGC1407	0.0060	23.27	265.6 ± 5.1	0.07 ± 0.003	N ^a	0.83 ± 0.06	41.92 ± 1.67	4.13 ± 0.25
NGC1521	0.0140	50.93	233.6 ± 8.9	0.07 ± 0.010	NE ^a	0.38 ± 0.39	20.90 ± 5.21	0.96 ± 0.83
NGC1600	0.0158	45.77	331.4 ± 7.0	0.07 ± 0.010	N ^a	0.72 ± 0.18	42.60 ± 7.16	5.07 ± 0.39
NGC2300	0.0064	41.45	266.0 ± 5.6	0.10 ± 0.010	N ^b	0.91 ± 0.13	26.09 ± 1.27	4.18 ± 0.43
NGC2305	0.0113	47.88	242.6 ± 13.4	0.19 ± 0.020	NE ^a	0.70 ± 0.25	20.22 ± 3.36	1.54 ± 0.58
NGC3091	0.0122	48.32	311.0 ± 7.7	0.20 ± 0.020	N ^a	0.40 ± 0.10	30.74 ± 4.16	3.48 ± 2.54
NGC3923	0.0058	20.97	245.6 ± 4.9	0.04 ± 0.001	N ^a	0.92 ± 0.12	21.98 ± 1.41	1.34 ± 0.12
NGC4073	0.0197	60.08	267.6 ± 6.3	1.05 ± 0.050	N ^a	0.61 ± 0.20	32.22 ± 2.92	8.30 ± 1.18
NGC4125	0.0045	21.41	239.8 ± 6.9	0.02 ± 0.001	U	0.13 ± 0.45	28.22 ± 12.35	1.43 ± 1.40
NGC4261	0.0073	29.58	296.7 ± 4.3	0.06 ± 0.003	NE ^{a,b}	1.16 ± 0.06	14.17 ± 1.47	0.52 ± 0.08
NGC4374	0.0033	16.68	277.6 ± 2.4	0.05 ± 0.002	NE ^a	1.18 ± 0.14	25.04 ± 6.58	1.86 ± 0.19
NGC4406	0.0006	16.08	231.4 ± 2.6	0.10 ± 0.004	E ^c	0.54 ± 0.14	26.28 ± 1.60	5.21 ± 3.26
NGC4472	0.0032	15.82	282.0 ± 2.9	0.16 ± 0.001	N ^a	0.96 ± 0.02	26.80 ± 0.23	1.17 ± 0.05
NGC4486	0.0042	16.56	323.0 ± 4.3	2.16 ± 0.004	E ^c	0.61 ± 0.01	22.73 ± 0.27	3.00 ± 0.10
NGC4552	0.0009	15.97	250.3 ± 2.9	0.03 ± 0.001	N ^a	0.95 ± 0.09	11.35 ± 0.63	2.23 ± 0.11
NGC4636	0.0031	15.96	199.5 ± 2.7	0.20 ± 0.002	NE ^a	1.00 ± 0.03	10.79 ± 0.36	1.89 ± 0.08
NGC4649	0.0034	16.55	330.5 ± 4.6	0.11 ± 0.002	N ^a	1.00 ± 0.02	22.63 ± 0.35	1.49 ± 0.02
NGC4696	0.0098	37.48	242.9 ± 6.5	2.49 ± 0.010	E ^c	0.69 ± 0.01	4.73 ± 0.03	2.24 ± 0.07
NGC4782	0.0133	48.63	310.0 ± 11.3	0.05 ± 0.010	NE ^{a,c}	0.59 ± 0.26	18.94 ± 9.92	4.30 ± 2.62
NGC5044	0.0090	35.75	224.9 ± 9.1	1.29 ± 0.010	E ^a	0.56 ± 0.03	5.75 ± 0.14	0.08 ± 0.12
NGC5419	0.0139	50.87	344.3 ± 5.4	0.24 ± 0.020	N ^a	1.19 ± 0.28	17.30 ± 2.21	1.38 ± 0.70
NGC5813	0.0064	29.23	236.0 ± 3.4	0.50 ± 0.003	E ^a	0.51 ± 0.02	12.20 ± 0.26	3.44 ± 0.13

^aClassification based on SOAR long-slit spectroscopy (T. Connor et al., in preparation).

^bClassification based on APO long-slit spectroscopy (M. Sun et al., in preparation).

^cSee Lakhchaura et al. (2018) for classification data source.

^dH α emission-line map from Hamer et al. (2016)

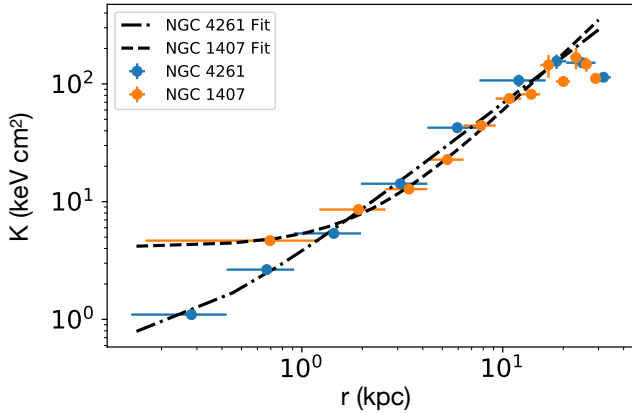


Figure 2. Examples of entropy profile fits. In NGC 4261 (blue points), the entropy profile is a nearly pure power law, so the best-fitting profile (dotted-dashed line) has a small value of K_0 . The entropy profile of NGC 1407 (orange points) has a significantly greater value of K_0 , reflected by the central flattening of its best-fitting entropy profile (dashed line).

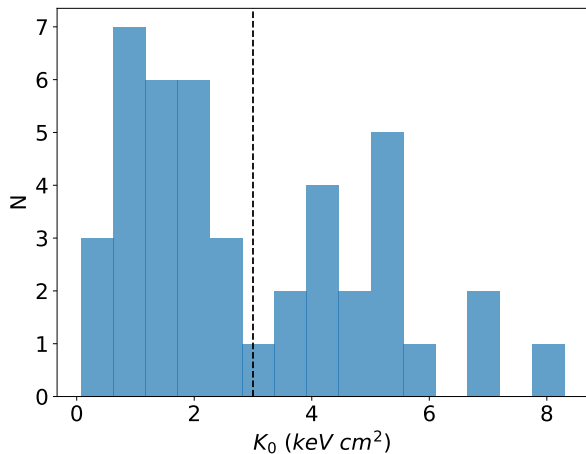


Figure 3. Distribution of K_0 values for the HQ subsample. The histogram shows K_0 values obtained by fitting Equation 2 in the 1–10 kpc radial interval to galaxies with sufficient spatial resolution. The black dashed vertical line at $K_0 = 3 \text{ keV cm}^2$ represents the criterion used to define the low K_0 subset.

We calculate the best-fit parameters using the Python package `emcee` (Foreman-Mackey et al. 2013). We establish an initial broad expected range for the parameters in log space with $0 < K_0 < 10^2$, $0 < K_{10} < 10^2$, and $0 < \alpha_K < 2$. Errors were determined from Markov Chain Monte Carlo (MCMC) contours in two dimensions (16 – 84%). Figure 2 shows two examples of entropy profile fits to high-quality data.

Our entropy profile fits suggest that approximately half of the HQ subsample is clustered near $K_0 \sim 1 - 2 \text{ keV cm}^2$, while the rest have $K_0 \gtrsim 3 \text{ keV cm}^2$ (see Fig-

ure 3). In the group with low K_0 , the entropy profile at 1–10 kpc is close to a pure power law. This set of galaxies is therefore more suitable for testing the prediction represented in Equation 1.

The subset with greater K_0 , by contrast, clearly deviates from the pure power-law entropy profile predicted by the basic analytical model. In those galaxies, central AGN heating may be producing an entropy floor at small radii, causing a flattening of the power-law profile that extends into the 1–10 kpc region. The best-fitting values of α_K in the high K_0 galaxies may still be representative of SN Ia heating, but the measurements of α_K are not as clean because of a greater degeneracy between K_0 and α_K in the fitting procedure.

2.4. Subset Selection

Our selection of the HQ subsample from the Lakhchaura et al. (2018) sample was intended to test the prediction described by Equation 1 as accurately as possible. Because the analysis requires a statistically significant measurement of the slope parameter α_K , the HQ subsample includes only those galaxies from Lakhchaura et al. (2018) with sufficient spatial resolution, defined to be at least 4 radial bins of any width in the 1–10 kpc radial interval. There are 36 galaxies in the Lakhchaura et al. (2018) sample that fit this criterion, and those are the ones making up the HQ subsample listed in Table 1.

Two further subsets of the Lakhchaura et al. (2018) sample are useful for the analysis in §3. The first is selected based on K_0 . Applying the cut at $K_0 = 3 \text{ keV cm}^2$ shown in Figure 3 defines a low K_0 subset of 22 galaxies that provide a cleaner test of the model predictions. A more restricted subset (hereafter referred to as the limited σ_v subset) is based on σ_v . It further limits the low K_0 subset to galaxies with $\sigma_v = 220\text{--}300 \text{ km s}^{-1}$. The rationale for focusing on that particular subset of 16 galaxies is discussed in Section 3.1.

3. DISCUSSION

3.1. Tests of the Analytical Prediction

The Voit et al. (2020) analytic model predicts a relationship for stellar velocity dispersion and entropy profile slope (Equation 1) in the radial range where SN Ia heating may be significant (within $\sim 1\text{--}10$ kpc). Elevated central entropy (K_0) beyond 1 kpc suggests that the central AGN is more strongly coupled to the surrounding medium at small radii (Prasad et al. 2020). Therefore, SN Ia heating may not be the only heating process at 1–10 kpc, in which case the simple analytical model does not strictly apply. Because the model presumes that AGN heating does not elevate the central entropy, we are motivated to investigate the relationship

between velocity dispersion and entropy profile slope in the low K_0 subset as well as the HQ subsample.

Table 2 summarizes the results of our exploration of the relationship between velocity dispersion and entropy profile slope for all three subsets defined in §2.4. To quantify the potential relationship between α_K and σ_v , we expand that relationship to linear order around the critical velocity dispersion to obtain the fitting formula

$$\alpha_K = \alpha_{240} + \alpha'_K(\sigma_{240} - 1) \quad (3)$$

where α_{240} is the best fit to α_K at $\sigma_v = 240 \text{ km s}^{-1}$, α'_K is the best-fitting slope of the σ_v - α_K relation in the vicinity of that point, and $\sigma_{240} \equiv \sigma_v/(240 \text{ km s}^{-1})$. We determine the best fits using an ordinary least squares method (Akritas & Bershady 1996), allowing for intrinsic scatter in α_K .

Figure 4 illustrates our results for the HQ subsample. Our linear fit gives $\alpha_{240} = 0.70 \pm 0.15$, consistent with the analytical prediction, with a slope of $\alpha'_K = 0.53 \pm 0.27$. While that slope differs from zero by only about 2σ , it represents tentative evidence for the predicted rise in α_K with σ_v , before the HQ subsample is further reduced. Therefore, limiting the radial range of the entropy profile fit and requiring sufficient data resolution over that radial range, as we have done here, help to reduce some of the ambiguity in the σ_v - α_K relation present in previous work (e.g. Babyk et al. 2018; Lakhchaura et al. 2018).

However, the HQ sample contains some galaxies that the analytical model of Voit et al. (2020) was not designed to describe. The low K_0 subset excludes many of those galaxies (see §2.4 for the rationale), and Figure 5 shows our fitting results for that subset. At 240 km s^{-1} , the best fit for α_K is essentially the same ($\alpha_{240} = 0.74 \pm 0.27$), but the slope of its dependence on σ_v is steeper ($\alpha'_K = 0.80 \pm 0.33$), providing stronger but not conclusive evidence for a positive σ_v - α_K correlation when the galaxies with elevated central entropy are removed.

Figure 5 also shows the best fit to the limited σ_v subset defined in §2.4. This subset excludes the single galaxy with $\sigma_v < 220 \text{ km s}^{-1}$ (NGC 4636, see §3.4.2) because the Voit et al. (2020) analytical model is not self-consistent for galaxies with σ_v much less than 240 km s^{-1} . The model assumes a steady outflow in which SN Ia exceeds radiative cooling everywhere. However, it predicts $\alpha_K < 2/3$ for $\sigma_v < 240 \text{ km s}^{-1}$, which leads to an inconsistency, because the ratio of SN Ia heating to radiative cooling then declines with increasing radius for $\alpha_K < 2/3$ (see Voit et al. 2020 for details). Consequently, such an atmosphere is prone to convective and thermal instabilities, because a cooling-dominated

region sits on top of a heating-dominated region. It is therefore unlikely to settle into a steady state like the one the model assumes. Instead, it should experience episodic feedback, fueled by intermittent accretion of multiphase gas, causing its entropy profile to fluctuate within a range spanning $5 < t_{\text{cool}}/t_{\text{ff}} < 20$ (see Prasad et al. 2020 for simulations demonstrating this behavior).

The limited σ_v subset also excludes the 5 galaxies from the low K_0 subset that have $\sigma_v > 300 \text{ km s}^{-1}$. There are two reasons for this restriction. First, the Voit et al. (2020) model assumes a singular isothermal sphere for the galaxy’s stellar mass profile (see Section 2.2), which results in an overprediction of α_K at large σ_v , relative to numerical integrations of more realistic models (see the dashed pink line in Figures 4). Second, some galaxies in the sample, like M87, are central galaxies in galaxy groups or clusters, and thus are in potential wells considerably deeper than indicated by the central galaxy’s stellar velocity dispersion. Consequently, they have greater circumgalactic gas pressure that does not allow SN Ia heating to drive the kind of outflow assumed by the analytic model. Applying an upper limit on stellar velocity dispersion therefore restricts the sample to galaxies most representative of the scenario the analytic model describes.

For this limited σ_v subset, we find best fits of $\alpha_{240} = 0.66 \pm 0.19$ and $\alpha'_K = 1.80 \pm 0.51$, which is more than $\sim 3\sigma$ away from a flat line. The criteria we have applied limit the subset to the galaxies most likely to follow the analytic model, so it is encouraging that the evidence for a relationship becomes stronger when the analysis focuses on galaxies with properties that are consistent with the analytical model’s assumptions. With these restrictions applied, the entropy profile slope appears to be much more closely connected to stellar velocity dispersion than indicated by previous works (e.g. Babyk et al. 2018; Lakhchaura et al. 2018). Also, the analytical prediction of equation (1), which has no free parameters, appears to match the σ_v - α_K relation observed among low K_0 early-type galaxies with $220 \text{ km s}^{-1} \lesssim \sigma_v \lesssim 300 \text{ km s}^{-1}$

3.2. Comparison to Numerical Predictions

Taken at face value, equation (1) implies that α_K increases without bound as σ_v rises and that it becomes infinite at a finite value of σ_v . Before that can happen, one or more of the assumptions in the analytical model must break down. The numerically integrated steady flow solutions presented in Voit et al. (2020) indicate that equation (1) indeed becomes increasingly invalid as σ_v rises above 300 km s^{-1} . That is because α_K at 1–10 kpc becomes increasingly sensitive to the effective

Table 2. Fits to the Observed Slope of the σ_v - α_K Relationship

Sample	α_{240}	α'_K	Reduced χ^2	Intrinsic Scatter	Number of Galaxies
High Quality (HQ)	0.70 ± 0.15	0.52 ± 0.24	1.03	0.18 ± 0.02	36
low K_0	0.74 ± 0.27	0.80 ± 0.33	1.05	0.22 ± 0.03	22
limited σ_v	0.66 ± 0.19	1.80 ± 0.51	1.08	0.16 ± 0.02	16

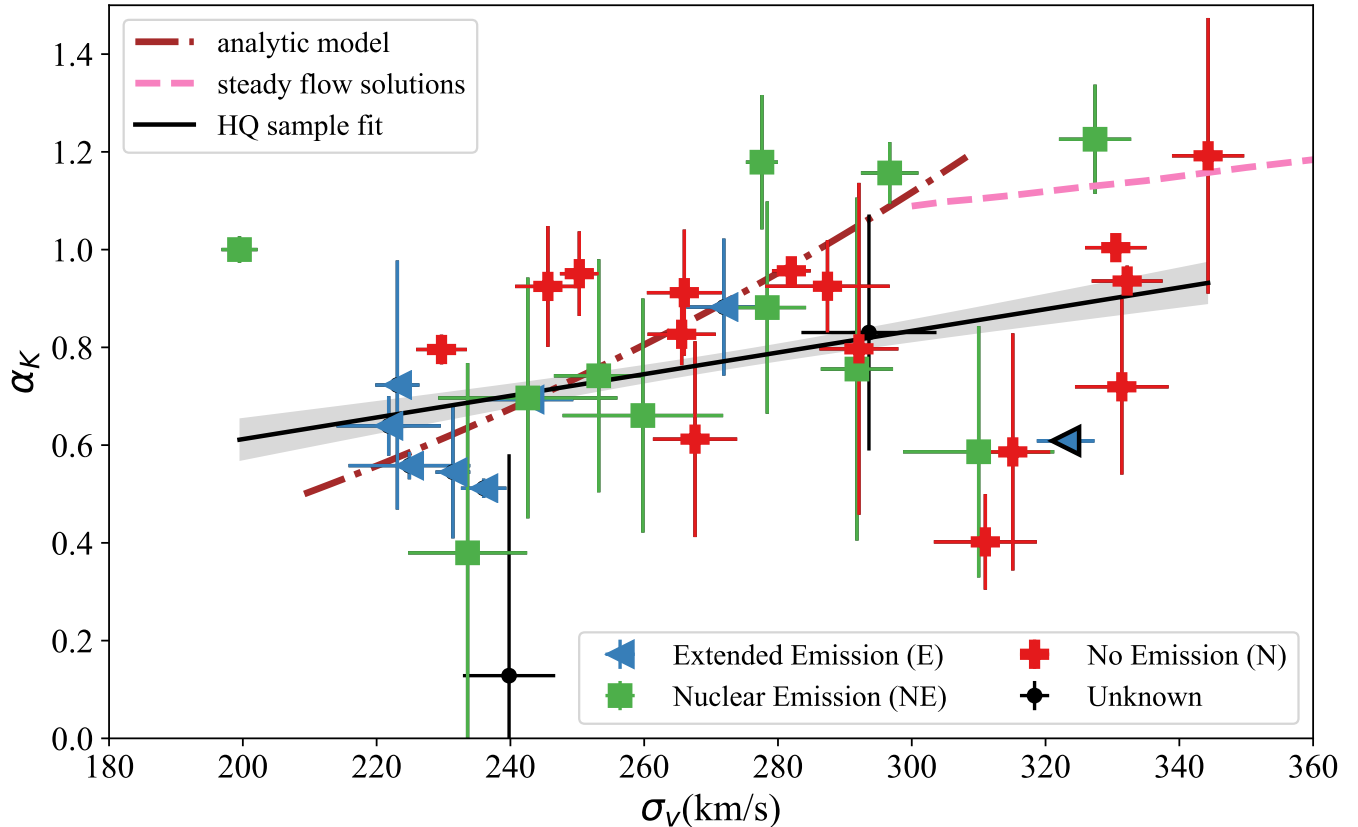


Figure 4. Stellar velocity dispersion vs. entropy profile slope for the HQ subsample of galaxies. Point colors and shapes represent multiphase gas extent as classified by Lakhchaura et al. (2018). Blue triangles are galaxies with extended multiphase gas (E), red crosses are galaxies with no extended multiphase gas (N), green squares are galaxies with multiphase gas contained within 2 kpc (NE), and black dots are galaxies without a gas extent classification. A black line shows the ordinary least squares fit to the data, with a gray band showing the 1σ error. A maroon dotted-dashed line represents the analytical prediction described by Equation 1. A pink dashed line represents the steady flow solutions for $\sigma_v \gtrsim 300 \text{ km s}^{-1}$ from Voit et al. (2020).

radius of the galaxy’s stellar mass distribution, which the simple analytical model does not account for. As a result, the numerically predicted entropy slope α_K levels off near 1.2, as indicated by the pink dashed lines in Figures 4 and 5. In practice, precise predictions for α_K in this range of σ_v require specification of the effective radius of the stellar mass distribution, introducing another galaxy parameter that is beyond the scope of this comparison.

Figure 5 shows that α_K in the low K_0 subset likewise levels off near 1.2 at $\sigma_v > 300 \text{ km s}^{-1}$. Among the five galaxies with $\sigma_v > 300 \text{ km s}^{-1}$, four have α_K between 0.9 and 1.2. The fifth is M87, which will be discussed separately in §3.4.1. The fact that the other four galaxies are close to the numerical model prediction but not the analytical prediction aligns with our rationale for truncating the low K_0 galaxies with $\sigma_v > 300 \text{ km s}^{-1}$ when defining the limited σ_v subset. However, additional observations of low K_0 galaxies with $\sigma_v > 300 \text{ km s}^{-1}$ are

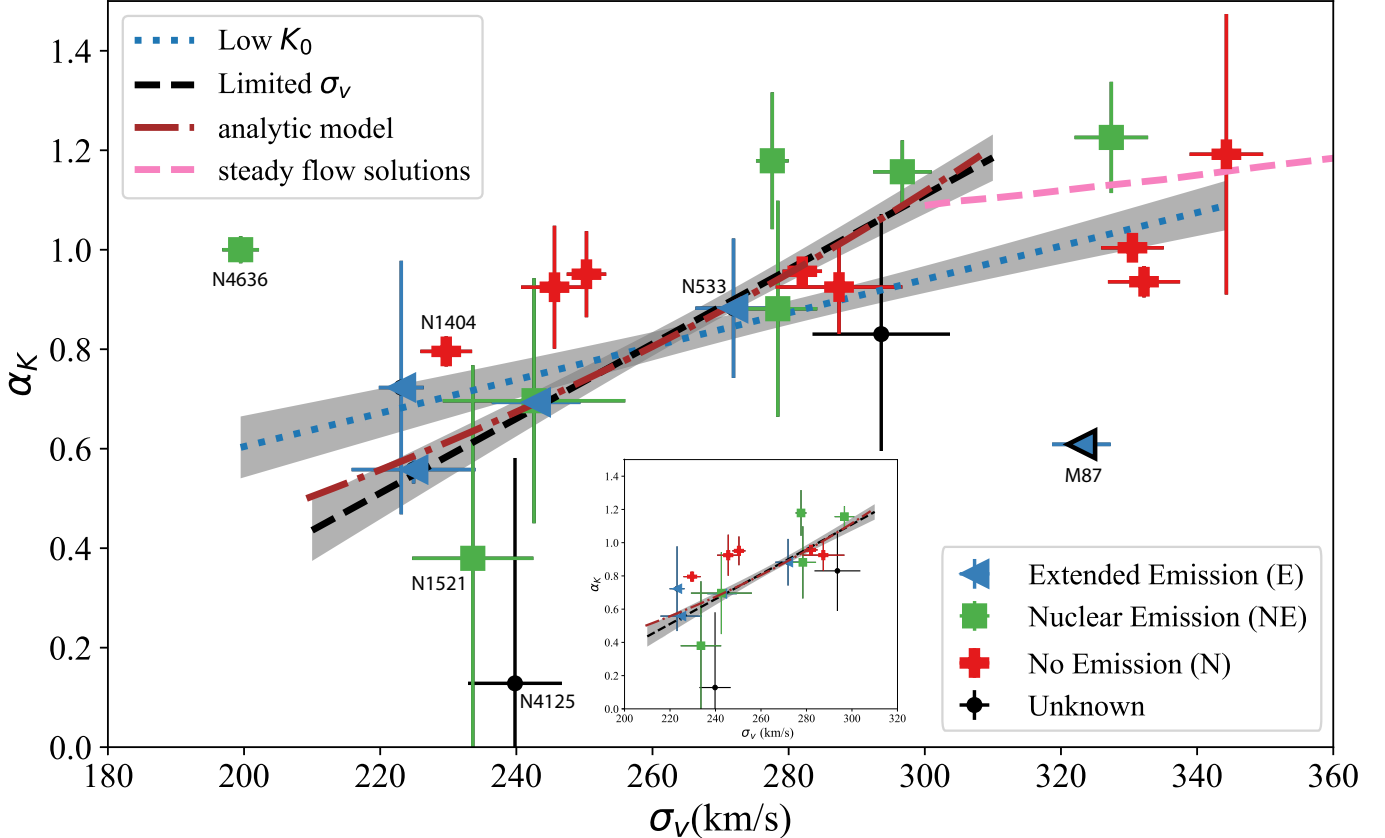


Figure 5. Stellar velocity dispersion vs. entropy profile slope for the low K_0 and restricted σ_v subsets. Points show the low K_0 subsample and are coded as in Figure 4. The dotted-dashed maroon and dashed pink lines are identical to the ones in Figure 4. A blue dotted line shows the best fit to the low K_0 sample, and a black dashed line shows the best fit to the limited σ_v sample, with gray bands representing 1σ errors. The inset shows just the restricted σ_v subset. The labeled galaxies are those galaxies discussed in §3.4.

needed to demonstrate more conclusively that the σ_v – α_K relation flattens as predicted by numerical models in the limit of $\sigma_v > 300 \text{ km s}^{-1}$.

3.3. Multiphase Gas Predictions

The black hole feedback valve model of Voit et al. (2020) also makes predictions for the extent of multiphase gas within an early-type galaxy. It predicts that extended multiphase gas should be prevalent among early-type galaxies with $\sigma_v \lesssim 240 \text{ km s}^{-1}$, which should also have $\alpha_K \lesssim 2/3$ and $5 \lesssim \min(t_{\text{cool}}/t_{\text{ff}}) \lesssim 20$. That prediction stems from the fact that $t_{\text{cool}}/t_{\text{ff}}$ declines with increasing radius for $\alpha_K \lesssim 2/3$, making the periphery of such a galaxy unstable to multiphase precipitation (see, e.g., Voit et al. 2017, 2020).

It also predicts that multiphase gas should become less extended and increasingly concentrated toward a galaxy’s center as σ_v increases, as long as the circumgalactic gas pressure is low enough for SN Ia heating to exceed radiative cooling within the galaxy. There are two reason for this concentration of multiphase gas to-

ward the center. First, the $t_{\text{cool}}/t_{\text{ff}}$ ratio of a galactic atmosphere with $\alpha_K > 2/3$ increases with increasing radius, meaning that the region of the atmosphere most prone to thermal instability is at small radii. Second, the ratio of SN Ia heating to radiative cooling within the galaxy also increases with radius for $\alpha_K > 2/3$, meaning that cooling is most likely to exceed heating at small radii. However, these predictions for correlations of multiphase gas extent with σ_v do not apply if the circumgalactic pressure is large enough for radiative cooling to exceed SN Ia heating within the galaxy, as in the central galaxies of galaxy clusters. In that case, AGN feedback is expected to maintain the central gas in a state with $5 \lesssim \min(t_{\text{cool}}/t_{\text{ff}}) \lesssim 20$ and $\alpha_K \approx 2/3$, which is marginally unstable to the production of extended multiphase gas.

Figures 6 and 7 present the relationships we find among multiphase gas extent, entropy profile slope at 1–10 kpc, and the minimum value of $t_{\text{cool}}/t_{\text{ff}}$ in the ambient galactic atmosphere. In making those figures, we have employed Kernel Density Estimation (KDE)

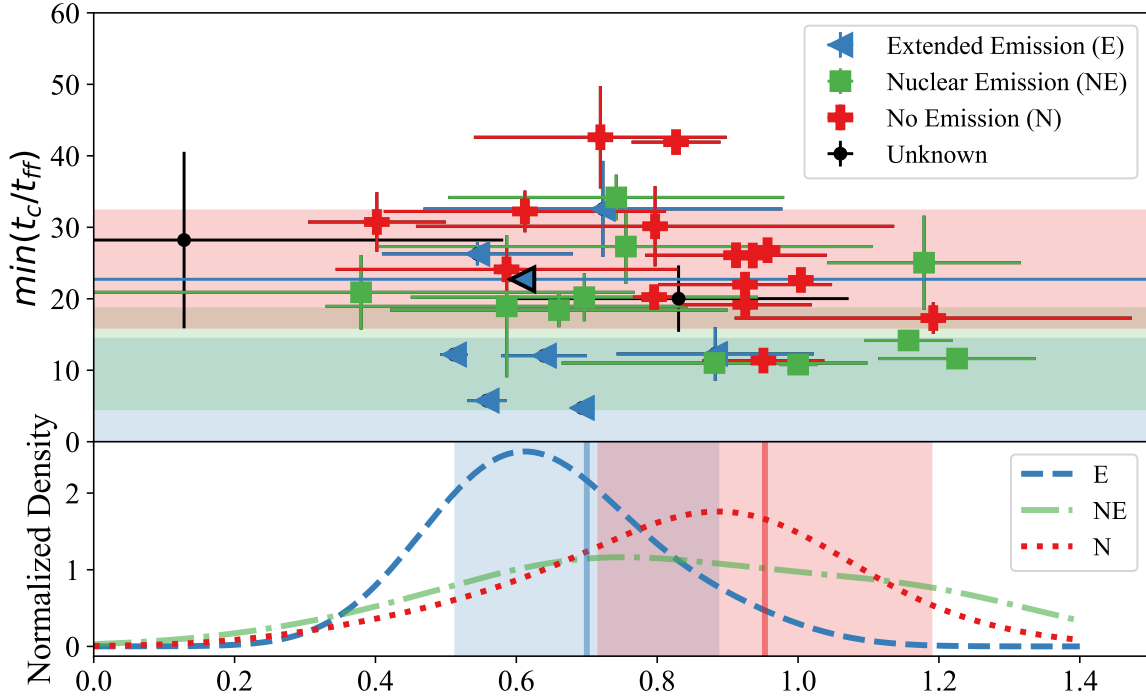


Figure 6. Dependence of multiphase gas extent on α_K and $\min(t_{\text{cool}}/t_{\text{ff}})$ in the HQ subsample. The top panel shows how the Lakhchaura et al. (2018) multiphase extent classification depends on both α_K and $\min(t_{\text{cool}}/t_{\text{ff}})$, with point colors and types as defined in Figure 4. The bottom panel shows the distribution of α_K values for each multiphase class, smoothed using gaussian Kernel Density Estimation (KDE). A blue dashed line shows galaxies with extended multiphase gas (E). A dotted-dashed green line shows galaxies with multiphase gas that does not extended beyond 2 kpc (NE). A dotted red line shows galaxies with no extended multiphase gas (N). The solid vertical lines correspond to the emission classifications in color and are the predicted α_K values calculated from Equation 1 using the average σ_v values for E (blue line) and N (red line) galaxies, with shading corresponding to the predicted dispersion in slope. Bandwidths used for KDE were E: 0.115, NE: 0.192, and N: 0.152.

to produce continuous distribution functions that express the dependence of multiphase gas extent on α_K . The KDE procedure convolves the discrete data with a smooth kernel function, in this case, a one-dimensional Gaussian with constant bandwidth. We chose KDE because it captures features of the distribution that could be masked by the choice of bin size in a histogram.

We chose a Gaussian kernel because the data are relatively simple and one dimensional. Bandwidths were determined for each multiphase gas extent category by minimizing the mean integrated square error (MISE):

$$\text{MISE}(\hat{f}_{\text{kern}}) = \mathbb{E} \left\{ \int [\hat{f}_{\text{kern}}(x) - f(x)]^2 dx \right\}, \quad (4)$$

where \hat{f}_{kern} is the chosen kernel function, \mathbb{E} represents the expectation value, and $f(x)$ is the underlying probability density function. For the KDE curves shown in the bottom panels of Figures 6 and 7, we used the

KDE tools from the `scikit-learn` Python package (Pedregosa et al. 2011).

Figure 6 shows results for the HQ subsample. The general trends for multiphase gas extent align with the model predictions, but the distributions of α_K are broad, especially in the NE and N categories. We find that galaxies with extended multiphase gas (E) tend to have entropy profile slopes close to $\alpha_K = 2/3$, as predicted, and single phase galaxies with no extended multiphase gas (N) tend to have greater values of α_K . However, the distribution function for the N galaxies significantly overlaps with the one for the E galaxies and extends below $\alpha_K = 0.5$. In the $\min(t_{\text{cool}}/t_{\text{ff}})$ dimension, we find that the E galaxies generally have the lowest values, mostly in the $5 \lesssim \min(t_{\text{cool}}/t_{\text{ff}}) \lesssim 20$ range. The N galaxies generally have the greatest values, mostly with $\min(t_{\text{cool}}/t_{\text{ff}}) > 20$, while the NE galaxies are intermediate between the other two categories. All of those

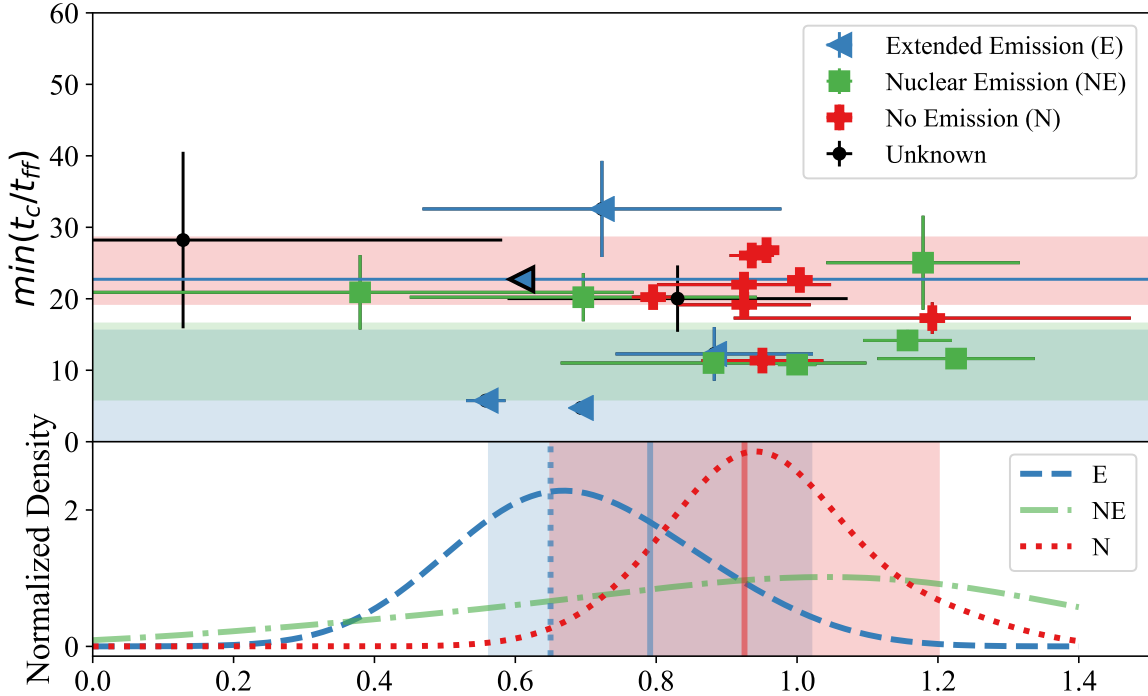


Figure 7. Dependence of multiphase gas extent on α_K and $\min(t_{\text{cool}}/t_{\text{ff}})$ in the low K_0 subset. The top panel shows how the Lakhchaura et al. (2018) multiphase extent classification depends on both α_K and $\min(t_{\text{cool}}/t_{\text{ff}})$, with point colors and types as defined in Figure 4. The bottom panel shows the distribution of α_K values for each multiphase class, smoothed using gaussian Kernel Density Estimation (KDE). The solid vertical lines are the predicted α_K values calculated using the average σ_v for E and N galaxies and Equation 1, and the dashed vertical line is the predicted α_K if M87 is removed from the multiphase galaxies. All figure elements have the same meanings as in Figure 6. Bandwidths used for KDE were E: 0.132, NE: 0.278, and N: 0.110.

findings are similar to those of Voit et al. (2015), but in a sample almost four times larger.

Two vertical lines in the bottom panel of Figure 6 show mean values of α_K predicted for the E and N galaxies by the simple analytical model. They were obtained by plugging the average value of σ_v for each galaxy population into equation (1). In both cases, the predicted value is close to the peak of the corresponding KDE curve.

Figure 7 shows results for the low K_0 subset. Note that removing the galaxies with elevated central entropy, which complicates measurements of α_K , has eliminated the set of single phase (N) galaxies with $\alpha_K \lesssim 2/3$. All of the remaining single phase galaxies have $\alpha_K \geq 0.8$, and they cluster near $\alpha_K \approx 1$. Likewise, many of the NE galaxies with low α_K have been pruned from the sample, shifting their mean value of α_K to well above $2/3$. Obtaining cleaner measurements of α_K by removing galaxies with $K_0 > 3 \text{ keV cm}^2$ has therefore sharpened the distribution functions in α_K . The galaxies with

extended multiphase gas are now clearly distinct from the other two sets in the α_K dimension and cluster near $\alpha_K \approx 2/3$, in agreement with model predictions.

Two solid vertical lines in the bottom panel of Figure 7 show predictions for α_K determined as in Figure 6 for the E and N galaxies by the simple analytical model. The red vertical line representing the prediction for the N galaxies is quite close to the peak of the corresponding KDE curve, but the blue vertical line representing the prediction for the E galaxies is now near $\alpha_K \approx 0.8$. This displacement of the prediction away from the peak of the KDE curve (near $\alpha_K \approx 2/3$) for the E galaxies is due entirely to M87, in which σ_v is much greater than in other four galaxies. Removing it from that set results in a prediction represented by the dotted blue line, which is much closer to the peak of the KDE curve, indicating good agreement with the analytical model.

3.4. Comments on Individual Galaxies

The comparisons shown in Figures 4 through 7 are encouraging for the black hole feedback valve model, but there are also some distinct outliers that disagree with the model’s predictions. The presence of outliers should not be surprising given the simplicity of the analytic model. We do not necessarily expect it to describe all galaxies, especially those in which something clearly more complex is happening. This section discusses some of the nonconforming galaxies among the low K_0 subset and considers characteristics of their environments that may explain why they do not conform.

3.4.1. M87

M87 (listed as NGC 4486 in Table 1) has $\sigma_v = 323.0 \pm 4.3$, $\alpha_K(1-10 \text{ kpc}) = 0.61 \pm 0.1$, and extended multiphase gas. Its low value of α_K , given the high σ_v , therefore makes it an outlier from the analytic model. However, its status as the central galaxy in a large potential well (the Virgo galaxy cluster) makes it unusual among the galaxies in the HQ subsample. The surrounding intracluster medium exerts a larger pressure on this galaxy’s atmosphere, causing radiative cooling to exceed SN Ia heating within the galaxy, thereby violating the assumptions on which equation (1) is based. Instead, we expect this galaxy’s atmosphere to be in a precipitation-limited state, with $\alpha_K \approx 2/3$, extended multiphase gas, and $5 \lesssim \min(t_{\text{cool}}/t_{\text{ff}}) \lesssim 20$. Its observed characteristics generally agree with those expectations, yet its $\min(t_{\text{cool}}/t_{\text{ff}}) = 22.73 \pm 0.27$ is slightly greater than expected for a galaxy with extended multiphase gas.

3.4.2. NGC 4636

NGC 4636 has $\sigma_v = 199.5 \pm 2.7$, $\alpha_K(1-10 \text{ kpc}) = 1.00 \pm 0.02$, $\min(t_{\text{cool}}/t_{\text{ff}}) = 10.79 \pm 0.36$, and multiphase gas that does not extend beyond 2 kpc. It is an outlier because its entropy slope is unusually large among the galaxies with $\sigma_v < 240 \text{ km s}^{-1}$. Voit et al. (2015) showed that this galaxy’s atmosphere is plausibly precipitation-limited, and Voit et al. (2020) pointed out that its inner entropy profile slope is consistent with that of a pure cooling flow (i.e. $\alpha_K = 1$). At $\sim 0.1 \text{ kpc}$, its entropy level reaches $\sim 1 \text{ keV cm}^2$, considerably below the level expected from $\sim 10^{42} \text{ erg s}^{-1}$ of intermittent kinetic feedback power (see Voit et al. 2020 for details).

There are several possible explanations for this low central entropy level: (1) time-averaged kinetic AGN power has been $\sim 10^{41} \text{ erg s}^{-1}$ for the last $\sim 100 \text{ Myr}$, (2) the AGN power has been highly collimated, as in NGC 4261, and has penetrated to $\gg 1 \text{ kpc}$ without dissipating much power, or (3) AGN power has been too weak to balance cooling for the last $\sim 100 \text{ Myr}$. In

this last case, a cooling catastrophe may be imminent, as suggested by the entropy profile between 0.5 and 2 kpc, and will soon trigger a strong feedback episode.

3.4.3. NGC 1521

NGC 1521 has $\sigma_v = 233.6 \pm 8.9$, $\alpha_K(1-10 \text{ kpc}) = 0.38 \pm 0.39$, $\min(t_{\text{cool}}/t_{\text{ff}}) = 20.90 \pm 0.51$, and multiphase gas that does not extend beyond 2 kpc. The best-fitting value of α_K is lower than the model prediction, but its uncertainty is large, most likely because of low spatial resolution. Its entropy profile has only four radial bins between 1 and 10 kpc, and one additional radial bin interior to 1 kpc. The resulting uncertainty does overlap the analytic prediction. Therefore, improved spatial resolution is necessary to determine if the galaxy does indeed conform to the model.

3.4.4. NGC 4125

NGC 4125 has $\sigma_v = 239.8 \pm 6.9$, $\alpha_K(1-10 \text{ kpc}) = 0.13 \pm 0.45$, and $\min(t_{\text{cool}}/t_{\text{ff}}) = 28.22 \pm 12.35$. Its multiphase gas classification is unknown. Like NGC 1521 its apparently shallow entropy slope, relative to the model prediction, may also result from poor spatial resolution. However, the shape of its entropy profile and some of its other characteristics are a bit more interesting. Its X-ray luminosity (measured inside 10 kpc) is the lowest in the HQ sample ($0.023 \pm 0.001 \times 10^{42} \text{ erg s}^{-1}$). Between 1 and 10 kpc, the entropy profile is almost flat, based on six radial bins. However, interior to 1 kpc, the entropy profile slope is much steeper, and Lakhchaura et al. (2018) find a power-law component in the X-ray spectrum, indicating the presence of an AGN with luminosity $0.006 \pm 0.001 \times 10^{41} \text{ erg s}^{-1}$. Wiklind et al. (1995) placed an upper limit on the molecular gas content, but the measurement is uncertain due to high systematic errors. The combination of the presence of an AGN, $\sigma_v < 240 \text{ km s}^{-1}$, and the flattened entropy profile at larger radii indicate that this may be a galaxy in which the steady flow is cooling-dominated at larger radii and prone to developing entropy inversions (Voit et al. 2020).

3.4.5. NGC 1404

NGC 1404 has $\sigma_v = 229.7 \pm 3.8$, $\alpha_K(1-10 \text{ kpc}) = 0.80 \pm 0.03$, $\min(t_{\text{cool}}/t_{\text{ff}}) = 20.23 \pm 0.51$, and no extended multiphase gas. It is notable as the only galaxy in the low K_0 subset with $\sigma_v < 240 \text{ km s}^{-1}$ and no multiphase gas. Aside from NGC 4636, it has the steepest entropy profile slope among the galaxies with $\sigma_v < 240 \text{ km s}^{-1}$, which may account for its lack of extended multiphase gas. Furthermore, its entropy profile sharply steepens beyond 7 kpc. It is a satellite of NGC 1399, and so the steep entropy gradient could potentially result from ram pressure stripping that truncates

the low-entropy outflow emanating from NGC 1404 as it orbits through the higher entropy intragroup medium around NGC 1399.

3.4.6. NGC 533

NGC 533 has $\sigma_v = 271.9 \pm 5.6$, $\alpha_K(1-10 \text{ kpc}) = 0.88 \pm 0.14$, $\min(t_{\text{cool}}/t_{\text{ff}}) = 12.28 \pm 3.75$, and extended multiphase gas. Along with M87, it is one of only two galaxies in the HQ sample with $\sigma_v > 245 \text{ km s}^{-1}$ that Lakhchaura et al. (2018) classified as E. But unlike M87, its entropy slope is completely consistent with the prediction of the simple analytical model. One reason for this blend of features may be that it is the central galaxy of a larger halo, like M87. According to Zabludoff & Mulchaey (1998), the velocity dispersion of the galaxies surrounding NGC 533 is $\sim 464 \text{ km s}^{-1}$. Furthermore, its low value of $\min(t_{\text{cool}}/t_{\text{ff}})$ suggests that the atmosphere of NGC 533 is susceptible to precipitation. It is also possible that NGC 533 is more similar to galaxies in the NE class, as its status as a galaxy with line emission extending beyond 2 kpc is marginal. The VIMOS map of that galaxy presented in Hamer et al. (2016) shows just a single small H α blob lying not far outside the 2 kpc radius limit that distinguishes NE galaxies from E galaxies.

3.5. Predictions for Profile Normalization

The analytical prediction from Voit et al. (2020) expressed in equation (1) presumes that SN Ia heating exceeds radiative cooling in the 1–10 kpc region. Figure 5 shows that the σ_v – α_K relationship observed in the low K_0 subset supports that prediction, especially in the interval $220 \text{ km s}^{-1} \leq \sigma_v \leq 300 \text{ km s}^{-1}$, and suggests another test of the model. For equation (1) to be a correct explanation for the σ_v – α_K relation, the normalizations of the pressure and density profiles in single phase galaxies must be consistent with an excess of SN Ia heating over radiative cooling at ~ 1 –10 kpc. This section assesses that prediction by comparing SN Ia heating with radiative cooling in the low K_0 subset using observed density and pressure profiles from Lakhchaura et al. (2018), focusing on the N and E galaxies.

According to the model, there is a critical gas pressure profile along which radiative cooling equals SN Ia heating:

$$P_{\text{eq}}(r) \equiv \left[\left(\epsilon_* + \frac{3}{2} \sigma_v^2 \right) \left(\frac{n^2}{n_e n_p} \right) \frac{\rho_*}{t_* \Lambda(T)} \right]^{1/2} kT . \quad (5)$$

This is Equation (11) from Voit et al. 2020, in which n_p is the proton density, ρ_* is the stellar mass density, t_*^{-1} is the specific stellar mass-loss rate, and $\Lambda(T)$ is the radiative cooling function. For the velocity dispersion

and temperature corresponding to the critical entropy profile slope ($\alpha_K = 2/3$ at $\sigma_v \approx 240 \text{ km s}^{-1}$), the model predicts $kT \approx 0.75 \text{ keV}$ and the critical pressure and density profiles for solar metallicity gas become:

$$P_{\text{eq}}(r) \approx (1.4 \times 10^{-10} \text{ erg cm}^{-3}) \sigma_{240}^3 r_{\text{kpc}}^{-1} \quad (6)$$

$$n_{e,\text{eq}} \approx (0.06 \text{ cm}^{-3}) \sigma_{240} r_{\text{kpc}}^{-1}, \quad (7)$$

where r_{kpc} is radius in kiloparsecs, if the weak dependence of $\Lambda(T)$ on σ_v is ignored (see equations 12 and 13 in Voit et al. 2020). Those expressions assume an isothermal stellar mass distribution ($\rho_* = \sigma_v/2\pi Gr^2$) and the fiducial values $\mu m_p \epsilon_* \approx 2 \text{ keV}$ and $t_* \approx 200 \text{ Gyr}$ (see Voit et al. 2020 for explanations of those fiducial values).

Figures 8 and 9 show comparisons of the extended multiphase (E) and single phase (N) galaxies in the HQ sample with the equilibrium pressure and density profiles from the model. Galaxies with multiphase gas confined to the central 2 kpc (NE) have been removed for clarity. If the model applies to the galaxies in the figure, then the equilibrium profiles derived from the model should divide the observed profiles of galaxies with extended multiphase gas (which typically have $\alpha_K \approx 2/3$) from those of galaxies with no extended multiphase gas (which typically have $\alpha_K \approx 1$). The black hole feedback valve model predicts that single phase galaxies (N) should have pressure profiles below P_{eq} at ~ 1 –10 kpc, while multiphase galaxies (E) should have pressure profiles above P_{eq} in that radial range.

The figures show that the equilibrium profiles (P_{eq} and $n_{e,\text{eq}}$) do indeed divide the HQ sample as predicted. However, there are two notable exceptions, one each among the multiphase and single phase galaxies: NGC 1316 and NGC 4073.

The multiphase galaxy NGC 1316 has a pressure profile that is close to P_{eq} within $\sim 1 \text{ kpc}$ but that drops below the P_{eq} locus at ~ 1 –4 kpc. It therefore has unusually low circumgalactic pressure for an early-type galaxy with extended multiphase gas. That said, it has apparently experienced a large feedback event during the last 0.5 Gyr (Lanz et al. 2010). Its radio and X-ray properties indicate that a kinetic feedback outburst of $\sim 5 \times 10^{58} \text{ ergs}$ occurred $\sim 0.4 \text{ Gyr}$ ago, producing large buoyant cavities in the galaxy’s hot atmosphere. Those cavities are now $\sim 100 \text{ kpc}$ from the center and may have stimulated production of extended multiphase gas through uplift (e.g., McNamara et al. 2016).

Conversely, the single phase galaxy NGC 4073 has one of the greatest X-ray luminosities in the HQ subsample, along with one of the hottest temperatures, and lies above the P_{eq} locus. It has $\alpha_K \approx 0.6$ and $\sigma_v \approx 268 \text{ km s}^{-1}$ and does not conform to the analytic

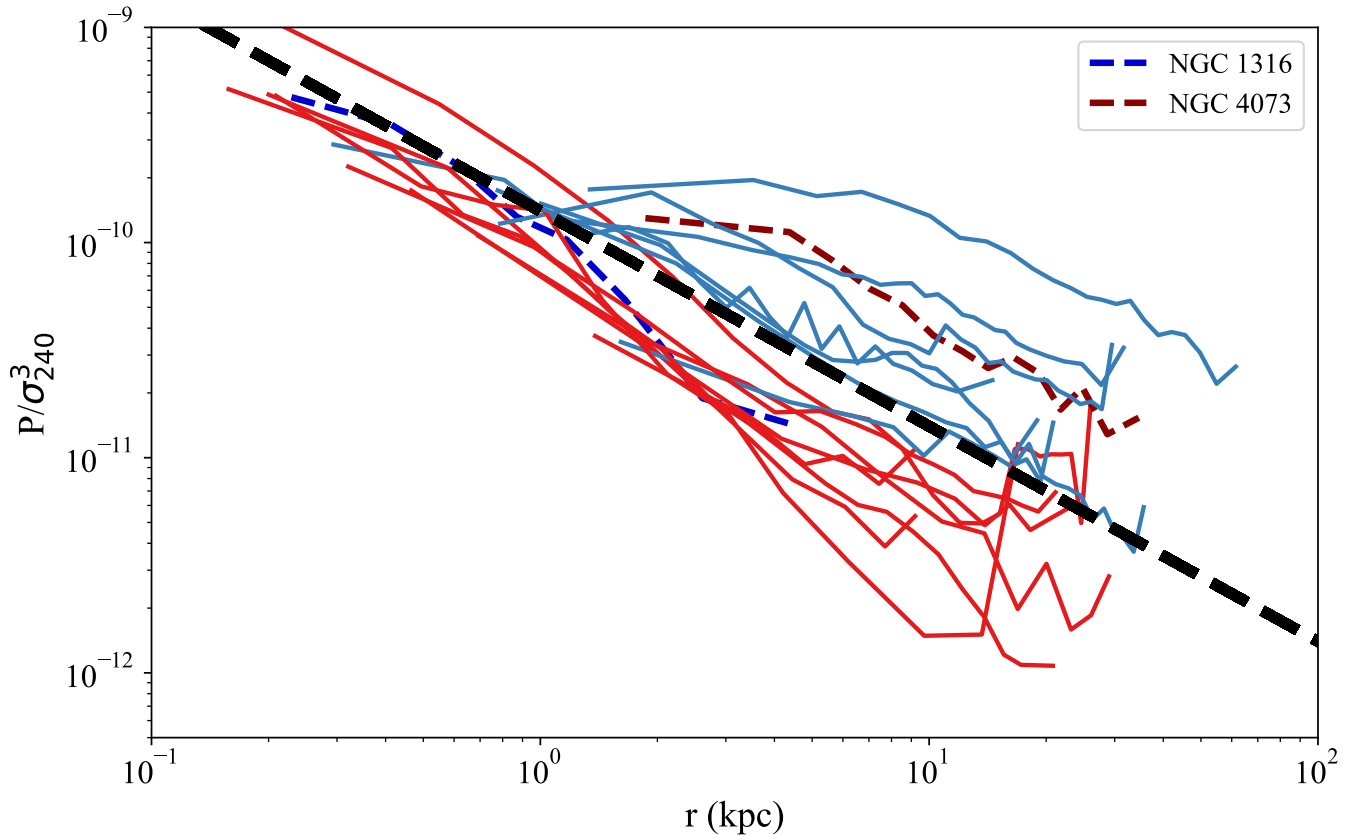


Figure 8. Scaled pressure profile comparisons for single phase and multiphase galaxies in the HQ subsample. A thick dashed black line shows the scaled pressure profile (P/σ_{240}^3) from equation (6), along which SN Ia heating should approximately balance radiative cooling. According to the model of Voit et al. (2020), galaxies with confining pressures greater than the line at ~ 10 kpc should be prone to precipitation and formation of extended multiphase gas, while galaxies with confining pressures below the line should be free of extended multiphase gas because of SN Ia-heated outflows that focus cooling and condensation within the central ~ 1 kpc. The observed pressure profiles of extended multiphase (E, blue lines) and single-phase (N, red lines) galaxies, shown without error bars for clarity, generally conform to that pattern. There are two exceptions in the HQ subsample: NGC 1316 (dark blue dashed line) and NGC 4073 (dark red dashed line). See Section 3.5 for discussions of these two galaxies.

model within the measurement uncertainty. However, it also has $\min(t_{\text{cool}}/t_{\text{ff}}) = 32.22 \pm 2.92$, which is large enough to strongly suppress multiphase condensation and would be an unusually large value of $\min(t_{\text{cool}}/t_{\text{ff}})$ for a galaxy with extended multiphase gas.

4. CONCLUSIONS

This paper has presented evidence for a relationship between stellar velocity dispersion σ_v and entropy profile slope α_K at 1–10 kpc in the Lakhchaura et al. (2018) sample of early-type galaxies. The characteristics of that relationship align with the predictions of the analytic model proposed by Voit et al. (2020), which has no free parameters. Furthermore, the significance of the result and its agreement with the analytic model improve as restrictions are placed on the sample to exclude galaxies that have properties inconsistent with the analytical model’s assumptions.

In contrast to previous studies of this type, we applied stricter limits on the data quality of the archival observations as well as limits on the characteristics of the galaxies being considered. Our HQ subsample of the Lakhchaura et al. (2018), which contains 36 galaxies, requires their radial entropy profiles to have at least three entropy bins in the 1–10 kpc range, outside of which the analytical model is not expected to apply. We measured the entropy profiles in that radial range by fitting the three-parameter model $K(r) = K_0 + K_{10}(r/10 \text{ kpc})^{\alpha_K}$. After obtaining those fits, we characterized the resulting σ_v – α_K relationship by fitting it with a two-parameter linear model. For the HQ subsample, we found $\alpha_K(240 \text{ km s}^{-1}) = 0.70 \pm 0.15$, in excellent agreement with the analytical prediction of $\alpha_K(240 \text{ km s}^{-1}) \approx 2/3$, along with evidence for a rise in α_K with σ_v at the $\approx 2\sigma$ level.

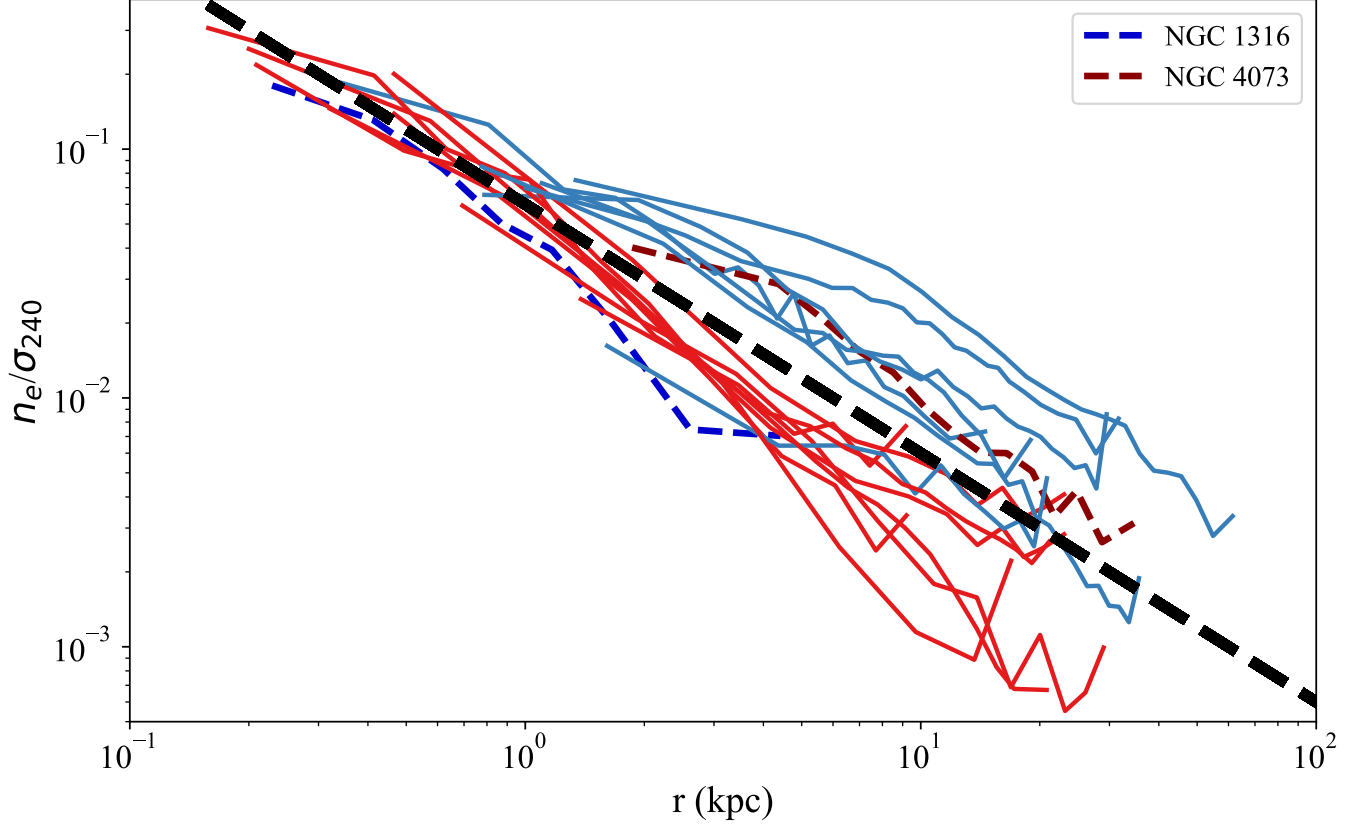


Figure 9. Scaled electron density comparisons for single phase and multiphase galaxies in the HQ subsample. A thick dashed black line shows the scaled electron density profile (n_e/σ_{240}) from equation (7), along which SN Ia heating should approximately balance radiative cooling. All other figure elements are as in Figure 8 and follow the same basic pattern, with low density allowing SN Ia heating to exceed radiative cooling in the 1–10 kpc range in single phase galaxies, while high density prevents SN Ia heating from exceeding radiative cooling in multiphase galaxies. NGC 1316 and NGC 4073 remain exceptions (see Section 3.5).

However, more than a third of the galaxies in the HQ subsample have $K_0 > 3 \text{ keV cm}^2$, a feature that compromises the fits for α_K and indicates that the 1–10 kpc region is heated by an AGN in addition to the SN Ia heating assumed by the analytical model. We therefore selected a low K_0 subset by excluding galaxies with $K_0 > 3 \text{ keV cm}^2$. Fitting a linear σ_v – α_K relationship to the remaining 22 galaxies gives $\alpha_K(240 \text{ km s}^{-1}) = 0.74 \pm 0.27$, consistent with the analytical prediction, and provides stronger evidence for a rise in α_K with σ_v at the 2.4σ level.

The final cut we made was to restrict the range of σ_v to galaxies for which the analytic model is most likely to be accurate. We excluded the one galaxy with $\sigma_v < 220 \text{ km s}^{-1}$, because the analytical model is not self-consistent there. We also excluded the five galaxies that have $K_0 < 3 \text{ keV cm}^2$ and $\sigma_v > 300 \text{ km s}^{-1}$ because the analytic predictions of Voit et al. (2020) overshoot their numerical predictions in that range of σ_v . For the remaining 16 galaxies we found $\alpha_K(240 \text{ km s}^{-1}) =$

0.66 ± 0.19 and more conclusive evidence for a rise in α_K with σ_v at the 3.5σ level. Furthermore, the best-fitting linear σ_v – α_K relationship is nearly identical to the analytic prediction.

The analytic model also successfully predicts how the normalizations of pressure and density profiles observed among galaxies with extended multiphase gas differ from the profiles observed among galaxies without extended multiphase gas. According to the model, galaxies with low circumgalactic pressure and high σ_v should be free of extended multiphase gas, while galaxies with high circumgalactic pressure should be precipitation-limited and prone to developing multiphase gas. The galaxies in our HQ subsample conform to that prediction with two exceptions: NGC 1316 and NGC 4073 (see Figures 8 and 9). NGC 1316 has an unusually low pressure at $< 10 \text{ kpc}$ for a multiphase galaxy but contains a powerful radio source (Fornax A). NGC 4073 has an unusually high pressure atmosphere for a galaxy without extended

multiphase gas but also has $t_{\text{cool}}/t_{\text{ff}} > 30$, which may account for the absence of a cooler gas phase.

Our work shows that while the Voit et al. (2020) analytic model may be overly idealized, it describes the relationship between key galaxy parameters well and can be used to further our understanding of how feedback in massive galaxies works. The comparison of the model to the data supports the notion that SN Ia heating plays an important role in the thermal evolution of massive galaxies. Furthermore, the relationship between entropy profile slope and velocity dispersion is highly dependent on the external gas pressure at larger radii. Current X-ray observations are not able to resolve pressure mea-

surements at large radii, but Athena and Lynx may be able to. Given the model predictions and existing observations, one could predict what the gas pressure at large radii should be and then test that prediction with the next generation of X-ray telescopes.

- 1 The scientific results reported in this article are based
- 2 on data obtained from the Chandra Data Archive. This
- 3 research has made use of software provided by the Chan-
- 4 dra X-ray Center in the applications package CIAO (Fr-
- 5 uscione et al. 2006). N.W. is supported by the GACR
- 6 grant 21-13491X.

REFERENCES

- Akritas, M. G. & Bershadsky, M. A. 1996, *ApJ*, 470, 706
- Babik, I. V., McNamara, B. R., Nulsen, P. E. J., et al. 2018, *ApJ*, 862, 39
- Boselli, A., Fossati, M., Longobardi, A., et al. 2019, *A&A*, 623, A52
- Cavagnolo, K. W., Donahue, M., Voit, G. M., & Sun, M. 2008, *ApJL*, 683, L107
- Dekel, A., Birnboim, Y., Engel, G., et al. 2009, *Nature*, 457, 451
- Donahue, M., Horner, D. J., Cavagnolo, K. W., & Voit, G. M. 2006, *ApJ*, 643, 730
- Donahue, M., Voit, G. M., O’Dea, C. P., Baum, S. A., & Sparks, W. B. 2005, *ApJL*, 630, L13
- Fabian, A. C. 1994, *ARA&A*, 32, 277
- Foreman-Mackey, D., Hogg, D. W., Lang, D., & Goodman, J. 2013, *PASP*, 125, 306
- Frisbie, R. L. S., Donahue, M., Voit, G. M., et al. 2020, *ApJ*, 899, 159
- Fruscione, A., McDowell, J. C., Allen, G. E., et al. 2006, in *Society of Photo-Optical Instrumentation Engineers (SPIE) Conference Series*, Vol. 6270, Society of Photo-Optical Instrumentation Engineers (SPIE) Conference Series, ed. D. R. Silva & R. E. Doxsey, 62701V
- Hamer, S. L., Edge, A. C., Swinbank, A. M., et al. 2016, *MNRAS*, 460, 1758
- Kereš, D., Katz, N., Davé, R., Fardal, M., & Weinberg, D. H. 2009, *MNRAS*, 396, 2332
- Kereš, D., Katz, N., Weinberg, D. H., & Davé, R. 2005, *MNRAS*, 363, 2
- Lakhchaura, K., Werner, N., Sun, M., et al. 2018, *MNRAS*, 481, 4472
- Lanz, L., Jones, C., Forman, W. R., et al. 2010, *ApJ*, 721, 1702
- Leitner, S. N. & Kravtsov, A. V. 2011, *ApJ*, 734, 48
- Mathews, W. G. & Brighenti, F. 2003, *ARA&A*, 41, 191
- McNamara, B. R. & Nulsen, P. E. J. 2007, *ARA&A*, 45, 117
- McNamara, B. R. & Nulsen, P. E. J. 2012, *New Journal of Physics*, 14, 055023
- McNamara, B. R., Russell, H. R., Nulsen, P. E. J., et al. 2016, *ApJ*, 830, 79
- Pedregosa, F., Varoquaux, G., Gramfort, A., et al. 2011, *Journal of Machine Learning Research*, 12, 2825
- Prasad, D., Voit, G. M., O’Shea, B. W., & Glines, F. 2020, *ApJ*, 905, 50
- Sparks, W. B., Donahue, M., Jordán, A., Ferrarese, L., & Côté, P. 2004, *ApJ*, 607, 294
- Voit, G. M. & Donahue, M. 2011, *ApJL*, 738, L24
- Voit, G. M., Donahue, M., O’Shea, B. W., et al. 2015, *ApJL*, 803, L21
- Voit, G. M., Meece, G., Li, Y., et al. 2017, *ApJ*, 845, 80
- Voit, G. M., Bryan, G. L., Prasad, D., et al. 2020, *ApJ*, 899, 70
- Werner, N., Allen, S. W., & Simionescu, A. 2012, *MNRAS*, 425, 2731
- Werner, N., McNamara, B. R., Churazov, E., & Scannapieco, E. 2019, *SSRv*, 215, 5
- Werner, N., Oonk, J. B. R., Sun, M., et al. 2014, *MNRAS*, 439, 2291
- White, S. D. M. & Frenk, C. S. 1991, *ApJ*, 379, 52
- Wiklind, T., Combes, F., & Henkel, C. 1995, *A&A*, 297, 643
- Zabludoff, A. I. & Mulchaey, J. S. 1998, *ApJ*, 496, 39